A comparison of three error estimation techniques for finite-volume solutions of compressible flows

C. Ilinca, X.D. Zhang, J.-Y. Trépanier *, R. Camarero

Centre de Recherche en Calcul Appliqué (CERCA), 5160, boul. Décarie, Suite 400, Montréal, Que., Canada H3X 2H9

Received 19 May 1999

Abstract

Three techniques to obtain error estimates for finite-volume solutions on unstructured grids are compared in this study. The first estimation technique uses Richardson extrapolation involving three flow solutions on different grids. Error estimates on these grids are computed simultaneously with the order of convergence. The second technique is based on the difference between the computed solution and a higher-order reconstruction obtained using the least-squares method. Finally, a third technique solves an error equation driven by source terms computed from the flux jump at cell interfaces. The flows solved as test cases are governed by the two-dimensional Euler equations, and the discretization employs Roe's flux difference splitting scheme. Comparisons with exact errors allow the efficiency of each error estimation technique to be assessed for various types of flows. © 2000 Published by Elsevier Science S.A.

1. Introduction

During recent decades, the coupled strategy of error estimation–mesh adaptation has been proposed as an efficient way to improve the accuracy of numerical solutions of partial differential equations. However, in the finite-volume community, most of the proposed adaptation strategies have been based on error indicators rather than on formal error estimators. There is now a consensus in the community that reliable error estimators must be developed. The present work is an attempt to present a step in this direction.

Our objective is to compare three error estimation techniques for the finite-volume solution of compressible flows governed by the Euler equations. The first technique is based on the classical Richardson extrapolation and involves the solution of the governing equations on three grids of different size [1,2]. The development is based on a Taylor series expansion of the solution as a function of the mesh size. This technique has the advantage of providing the order of convergence of the method as a by-product.

The second error estimation technique is based on a higher-order reconstruction of the solution and provides a measure of the interpolation error. The technique bears some relationship to the interpolation error estimators used in the finite-element community for elliptic problems [3,4]. For the finite-volume method, error estimations by solution reconstruction can be found in Ref. [5]. However, its application to hyperbolic problems has not been validated and is the subject of debate.

The third error estimation technique has been specifically designed for hyperbolic problems and has been tailored for the numerical scheme used [6,7]. It is based on the solution of a linear hyperbolic error equation which is derived from the original system of equations. Error source terms are obtained by the analysis of the scheme with the modified equation approach.

---

* Corresponding author.

Test cases with known analytical solutions have been selected to allow a quantitative comparison of the global and local performance of the error estimators. A rigorous comparison of these three techniques will be performed for smooth subsonic and supersonic flows and for a supersonic flow with discontinuities. As a last case, the methods will be compared for a transonic airfoil flow.

2. Governing equations

The Euler equations form a non-linear hyperbolic system of conservation laws representing the most accurate model for compressible inviscid flows. Continuity, momentum and energy conservations are given by:

$$\frac{\partial \mathbf{U}}{\partial t} + \frac{\partial \mathbf{f}}{\partial x} + \frac{\partial \mathbf{g}}{\partial y} = 0, \tag{1}$$

where the vector of conserved variables $\mathbf{U}$ is defined by:

$$\mathbf{U} = \begin{bmatrix} \rho \\ \rho u \\ \rho v \\ \rho E_t \end{bmatrix}, \tag{2}$$

and the convective fluxes $\mathbf{f}$ and $\mathbf{g}$ are given by:

$$\mathbf{f} = \begin{bmatrix} \rho u \\ \rho u^2 + p \\ \rho u v \\ (\rho E_t + p)u \end{bmatrix}, \quad \mathbf{g} = \begin{bmatrix} \rho v \\ \rho u v \\ \rho v^2 + p \\ (\rho E_t + p)v \end{bmatrix}. \tag{3}$$

The system is closed by the equation of state for a perfect gas:

$$p = (\gamma - 1) \left[\rho E_t - \frac{(\rho u)^2 + (\rho v)^2}{2\rho} \right], \tag{4}$$

where ρ represents the density, u and v the velocity components in the x and y directions respectively, E_t the total energy by unit of mass, and p the static pressure. γ is the ratio of the specific heats, $\gamma = c_p/c_v$, and has a value of 1.4.

These equations are solved using a finite-volume upwind scheme on triangular grids, as proposed in Refs. [8,9]. In the compressible flow regime, most finite-volume schemes are collocated. In the present work, the conserved variables $\mathbf{U}$ are stored at the center of each triangle. The second-order scheme use a higher-order reconstruction of the solution based on the least-squares technique [10].

3. Error estimation by Richardson extrapolation

The first step in evaluating the error using Richardson extrapolation is to determine the order of convergence of the solver. For a problem having a known analytical solution, the order of convergence is found by a grid refinement study [11,12]. Considering two grids with elements of size $t^{(1)}$ and $t^{(2)}$, where $t^{(2)} = 2t^{(1)}$, the global error of the numerical solution $\mathbf{U}$ is measured by the L_2 norm, as defined by the following relation:

$$E = \|\mathbf{U} - \mathbf{U}_{\text{ex}}\| = \sqrt{\int_V (\mathbf{U} - \mathbf{U}_{\text{ex}})^2 \, d\Omega}. \tag{5}$$

Here $\mathbf{U}$ and $\mathbf{U}_{\text{ex}}$ are the numerical and exact solutions, respectively. Assuming that the error is of order $\mathbf{p}$, one can write:

$$E^{(1)} = \|\mathbf{U}^{(1)} - \mathbf{U}_{\text{ex}}\| = C\big[t^{(1)}\big]^{\mathbf{p}}, \tag{6}$$

$$E^{(2)} = \|\mathbf{U}^{(2)} - \mathbf{U}_{\text{ex}}\| = C\big[t^{(2)}\big]^{\mathbf{p}} \tag{7}$$

with C a constant.

Consequently, the order of convergence may be written as:

$$\mathbf{p} = \frac{\ln\left(\frac{\|\mathbf{U}^{(1)} - \mathbf{U}_{\text{ex}}\|}{\|\mathbf{U}^{(2)} - \mathbf{U}_{\text{ex}}\|}\right)}{\ln\left(\frac{t^{(1)}}{t^{(2)}}\right)}. \tag{8}$$

For a problem without a known analytical solution, Roache [1] suggests a method based on a posteriori evaluation of the convergence rate based on a grid refinement study. The convergence rate is established using three solutions $\mathbf{U}^{(1)}, \mathbf{U}^{(2)}, \mathbf{U}^{(3)}$ on different grids, with $\mathbf{U}^{(1)}$ representing the solution on the finest grid. For a constant refinement factor $r = t^{(2)}/t^{(1)} = t^{(3)}/t^{(2)}$, the estimated convergence rate is:

$$\mathbf{p} = \ln\left(\frac{\|\mathbf{U}^{(3)} - \mathbf{U}^{(2)}\|}{\|\mathbf{U}^{(2)} - \mathbf{U}^{(1)}\|}\right)\frac{1}{\ln(r)}, \tag{9}$$

where $\|\mathbf{U}^{(3)} - \mathbf{U}^{(2)}\|$ and $\|\mathbf{U}^{(2)} - \mathbf{U}^{(1)}\|$ represent the L_2 norms of the difference between the solutions $\mathbf{U}^{(3)}$ and $\mathbf{U}^{(2)}$, $\mathbf{U}^{(2)}$ and $\mathbf{U}^{(1)}$, respectively, as given by:

$$\|\mathbf{U}^{(3)} - \mathbf{U}^{(2)}\| = \sqrt{\int_V (\mathbf{U}^{(3)} - \mathbf{U}^{(2)})^2 \, d\Omega}, \tag{10}$$

$$\|\mathbf{U}^{(2)} - \mathbf{U}^{(1)}\| = \sqrt{\int_V (\mathbf{U}^{(2)} - \mathbf{U}^{(1)})^2 \, d\Omega}, \tag{11}$$

Once the order of convergence is known, the error estimation based on Richardson's extrapolation starts from a Taylor series representation of the discrete solution $\mathbf{U}$:

$$\mathbf{U} = \mathbf{U}_{\text{ex}} + a_1 t + a_2 t^2 + a_3 t^3 + \cdots, \tag{12}$$

where t is the grid size and a_i are grid-independent coefficients in the asymptotic region. $\mathbf{U}_{\text{ex}}$ can be approximated for first- and second-order schemes as a result of mathematical manipulations of relation (12) written for two solutions on different grids $\mathbf{U}^{(1)}$ and $\mathbf{U}^{(2)}$ as:

$$\mathbf{U}_{\text{ex}}^{\text{1st order}} = \mathbf{U}^{(1)} + \frac{\mathbf{U}^{(1)} - \mathbf{U}^{(2)}}{r - 1} + \mathbf{O}(2), \tag{13}$$

$$\mathbf{U}_{\text{ex}}^{\text{2nd order}} = \mathbf{U}^{(1)} + \frac{\mathbf{U}^{(1)} - \mathbf{U}^{(2)}}{r^2 - 1} + \mathbf{O}(3), \tag{14}$$

where $r = t^{(2)}/t^{(1)}$ is the refinement factor. This can be generalized for a $\mathbf{p}$-order method, expressions (13) and (14) being replaced by:

$$\mathbf{U}_{\text{ex}}^{\mathbf{p}-\text{order}} = \mathbf{U}^{(1)} + \frac{\mathbf{U}^{(1)} - \mathbf{U}^{(2)}}{r^{\mathbf{p}} - 1}. \tag{15}$$

Consequently, the error estimates on the medium and the fine grid are respectively:

$$e^{(2)} = \frac{r^{\mathbf{p}}\|\mathbf{U}^{(2)} - \mathbf{U}^{(1)}\|}{|1 - r^{\mathbf{p}}|} \approx \|\mathbf{U}^{(2)} - \mathbf{U}_{\text{ex}}\|, \tag{16}$$

$$e^{(1)} = \frac{\|\mathbf{U}^{(2)} - \mathbf{U}^{(1)}\|}{|1 - r^{\mathbf{p}}|} \approx \|\mathbf{U}^{(1)} - \mathbf{U}_{\text{ex}}\|. \tag{17}$$

As the order of the method varies with the type of application, the error estimates must be computed using the estimated convergence rate $\mathbf{p}$ instead of its formal value.

4. Error estimation by solution reconstruction

This method is based on the difference between the computed solution and a reconstructed higher-order solution. Let $\mathbf{U}_{\text{ex}}$ and $\mathbf{U}$ be the exact and finite-volume solutions, respectively. The true error is $E = \|\mathbf{U}_{\text{ex}} - \mathbf{U}\|$ measured in some appropriate norm.

In cases of practical interest, $\mathbf{U}_{\text{ex}}$ is not known and is replaced by an approximation $\mathbf{U}^*$ which must be of higher accuracy than $\mathbf{U}$. The error estimator is then given by $e = \|\mathbf{U}^* - \mathbf{U}\|$.

A weighted least-squares procedure is used to obtain an approximation of the derivatives [13]. First, we will focus on a piecewise linear reconstruction of a piecewise constant solution. In this case, the reconstruction $\mathbf{U}_i^*$ is given by:

$$\mathbf{U}_i^*(x, y) = \mathbf{U}_i^0 + \Delta x \, \mathbf{U}_x + \Delta y \, \mathbf{U}_y, \tag{18}$$

where $\mathbf{U}_i^0$ is the piecewise constant solution located at the centroid of the element i.

The computation of the derivatives at the center of the element i involves all its n neighbors (see Fig. 1). The system to solve is:

$$\begin{bmatrix} \sum_{j=1}^n \Delta x_j^2 \, w_j^2 & \sum_{j=1}^n \Delta x_j \, \Delta y_j \, w_j^2 \\ \sum_{j=1}^n \Delta x_j \, \Delta y_j \, w_j^2 & \sum_{j=1}^n \Delta y_j^2 \, w_j^2 \end{bmatrix} \begin{bmatrix} \mathbf{U}_x \\ \mathbf{U}_y \end{bmatrix} = \begin{bmatrix} \sum_{j=1}^n \Delta x_j \, \Delta \mathbf{U}_j \, w_j^2 \\ \sum_{j=1}^n \Delta y_j \, \Delta \mathbf{U}_j \, w_j^2 \end{bmatrix}, \tag{19}$$

where $\Delta \mathbf{U}_j \equiv \mathbf{U}_j - \mathbf{U}_i$, $\Delta x_j \equiv x_j - x_i$, $\Delta y_j \equiv y_j - y_i$ and w_j is a geometric weight introduced in order to account for the relative position of every neighbor. For $\mathbf{U}_x$ and $\mathbf{U}_y$, the subscripts denote partial derivatives at (x_i, y_i), the center of element i. More details concerning this procedure can be found in Refs. [10,13].

Once the gradients $\mathbf{U}_x$ and $\mathbf{U}_y$ are computed, the reconstructed solution at a point of coordinates (x, y) is given by Eq. (18).

The error e_i associated with the mesh element i is estimated as the L_2 norm of the difference between the reconstructed piecewise linear and the computed piecewise constant solutions:
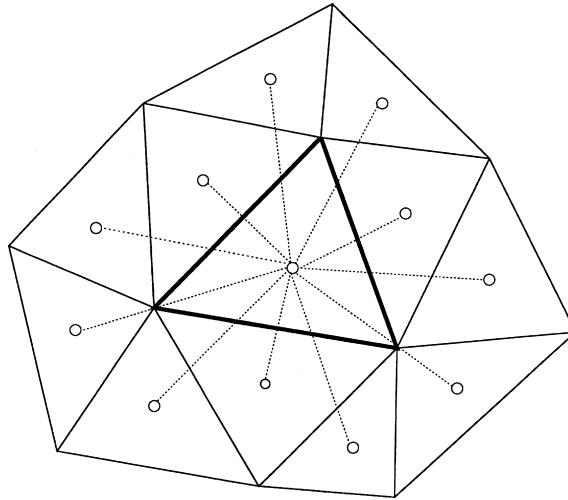

Fig. 1. The central triangular finite-volume i and its neighbors.

$$e_i = \|\mathbf{U}^*(x,y) - \mathbf{U}\|_i = \sqrt{\int_{V_i} \left(\mathbf{U}_i^*(x,y) - \mathbf{U}_i\right)^2 \, \mathrm{d}V}. \tag{20}$$

Knowing that for the piecewise linear solution $\mathbf{U}_i = \mathbf{U}_i^0$, Eq. (20) becomes:

$$e_i = \sqrt{\int_{V_i} \left(\mathbf{U}_i^*(x,y) - \mathbf{U}_i^0\right)^2 \, \mathrm{d}V} = \sqrt{\int_{V_i} \left(\Delta x \mathbf{U}_x + \Delta y \mathbf{U}_y\right)^2 \, \mathrm{d}V}. \tag{21}$$

Finally, the global L_2 norm of the error is simply given by:

$$e = \sqrt{\sum_{i=1}^{N} e_i^2}. \tag{22}$$

To avoid possible errors from the evaluation of integrals, these have been computed using a Gauss quadrature with 19 points in the present work.

For the second-order scheme, two different reconstructions are computed. The least-squares technique is used to perform the reconstruction, both for the piecewise linear solution $\mathbf{U}$ and the piecewise quadratic one, $\mathbf{U}^*$. Following the procedure presented in the previous section, the piecewise linear solution is assumed to take the form:

$$\mathbf{U}_i(x,y) = \mathbf{U}_i^0 + \Delta x \, \mathbf{U}_x + \Delta y \, \mathbf{U}_y, \tag{23}$$

where the superscript 0 denotes the finite-volume average solution at the centroid of the triangle i. $\mathbf{U}_x$ and $\mathbf{U}_y$ in Eq. (23) are computed as in (19).

A least-squares procedure is also used to compute the reconstructed piecewise quadratic solution. The system to solve is $[\mathbf{L}][\mathbf{X}] = [\mathbf{R}]$, where the left-hand side is given by:

$$[\mathbf{L}] = \begin{bmatrix} \sum_{j=1}^{n} \Delta x_j^2 & \sum_{j=1}^{n} \Delta x_j \, \Delta y_j & \frac{1}{2}\sum_{j=1}^{n} \Delta x_j^3 & \sum_{j=1}^{n} \Delta x_j^2 \, \Delta y_j & \frac{1}{2}\sum_{j=1}^{n} \Delta x_j \, \Delta y_j^2 \\ \sum_{j=1}^{n} \Delta x_j \, \Delta y_j & \sum_{j=1}^{n} \Delta y_j^2 & \frac{1}{2}\sum_{j=1}^{n} \Delta x_j^2 \, \Delta y_j & \sum_{j=1}^{n} \Delta x_j \, \Delta y_j^2 & \frac{1}{2}\sum_{j=1}^{n} \Delta y_j^3 \\ \frac{1}{2}\sum_{j=1}^{n} \Delta x_j^3 & \frac{1}{2}\sum_{j=1}^{n} \Delta x_j^2 \, \Delta y_j & \frac{1}{4}\sum_{j=1}^{n} \Delta x_j^4 & \frac{1}{2}\sum_{j=1}^{n} \Delta x_j^3 \, \Delta y_j & \frac{1}{4}\sum_{j=1}^{n} \Delta x_j^2 \, \Delta y_j^2 \\ \sum_{j=1}^{n} \Delta x_j^2 \, \Delta y_j & \sum_{j=1}^{n} \Delta x_j \, \Delta y_j^2 & \frac{1}{2}\sum_{j=1}^{n} \Delta x_j^3 \, \Delta y_j & \sum_{j=1}^{n} \Delta x_j^2 \, \Delta y_j^2 & \frac{1}{2}\sum_{j=1}^{n} \Delta x_j \, \Delta y_j^3 \\ \frac{1}{2}\sum_{j=1}^{n} \Delta x_j \, \Delta y_j^2 & \sum_{j=1}^{n} \Delta y_j^3 & \frac{1}{4}\sum_{j=1}^{n} \Delta x_j^2 \, \Delta y_j^2 & \frac{1}{2}\sum_{j=1}^{n} \Delta x_j \, \Delta y_j^3 & \frac{1}{4}\sum_{j=1}^{n} \Delta y_j^4 \end{bmatrix} \tag{24}$$

and the right-hand side can be written as follows:

$$[\mathbf{R}] = \begin{bmatrix} \sum_{j=1}^{n} \Delta x_j \, \Delta\mathbf{U}_j \\ \sum_{j=1}^{n} \Delta y_j \, \Delta\mathbf{U}_j \\ \frac{1}{2}\sum_{j=1}^{n} \Delta x_j^2 \, \Delta\mathbf{U}_j \\ \sum_{j=1}^{n} \Delta x_j \, \Delta y_j \, \Delta\mathbf{U}_j \\ \frac{1}{2}\sum_{j=1}^{n} \Delta y_j^2 \, \Delta\mathbf{U}_j \end{bmatrix}. \tag{25}$$

As for the piecewise linear reconstruction, more details can be found in Refs. [10,13]. Once the unknown vector $[\mathbf{X}] = [\mathbf{U}_x, \mathbf{U}_y, \mathbf{U}_{xx}, \mathbf{U}_{xy}, \mathbf{U}_{yy}]^\mathrm{T}$ is computed, the reconstructed piecewise quadratic solution is given by:

$$\mathbf{U}_i^*(x,y) = \mathbf{U}_i^0 + \Delta x \, \mathbf{U}_x + \Delta y \, \mathbf{U}_y + \frac{(\Delta x)^2}{2} \mathbf{U}_{xx} + \frac{(\Delta y)^2}{2} \mathbf{U}_{yy} + (\Delta x)(\Delta y)\mathbf{U}_{xy}. \tag{26}$$

The error estimator is then given by $e_i = \|\mathbf{U}_i^*(x,y) - \mathbf{U}_i(x,y)\|$, where $\mathbf{U}_i^*(x,y)$ and $\mathbf{U}_i(x,y)$ are defined by relations (26) and (23), respectively. The global L_2 norm of the error can be computed using (22).

5. Error estimation by error equation

A procedure for a posteriori error estimation for hyperbolic conservation laws has been proposed by Zhang et al. [6] for one-dimensional problems. A two-dimensional extension of this technique can be found in Ref. [7]. This method is based on solving linearized hyperbolic equations for the errors with source terms obtained using modified equation analysis [14,15]. The dominant term in the modified equation is used as the error source. This provides an alternative way of estimating the solution error for hyperbolic equations. This technique accounts for the wave structure of the solution. In particular, it will detect convection of errors, which is a non-local phenomenon.

Considering the Euler equations given by Eq. (1) and their finite-volume approximation $\mathbf{U}$, the following residual can be defined:

$$\frac{\partial \mathbf{U}}{\partial t} + \frac{\partial \mathbf{f}(\mathbf{U})}{\partial x} + \frac{\partial \mathbf{g}(\mathbf{U})}{\partial y} = \mathbf{r}(\mathbf{U}). \tag{27}$$

Defining the error vector as $\mathbf{E} = \mathbf{U}_{\mathrm{ex}} - \mathbf{U}$ and subtracting Eq. (27) from Eq. (1), one obtains:

$$\frac{\partial \mathbf{E}}{\partial t} + \frac{\partial}{\partial x}[\tilde{A}(\mathbf{U}_{\mathrm{ex}}, \mathbf{U})\mathbf{E}] + \frac{\partial}{\partial y}[\tilde{B}(\mathbf{U}_{\mathrm{ex}}, \mathbf{U})\mathbf{E}] = -\mathbf{r}(\mathbf{U}), \tag{28}$$

where

$$A = \frac{\partial \mathbf{f}}{\partial \mathbf{U}_{\mathrm{ex}}}, \quad B = \frac{\partial \mathbf{g}}{\partial \mathbf{U}_{\mathrm{ex}}}$$

are the Jacobian matrices, and the *tilde* represents Roe's averaging based on two states. In practice, it is reasonable to replace $\mathbf{U}_{\mathrm{ex}}$ by $\mathbf{U}$ in the Jacobian matrices, and Eq. (28) becomes

$$\frac{\partial \mathbf{E}}{\partial t} + \frac{\partial}{\partial x}[A(\mathbf{U})\mathbf{E}] + \frac{\partial}{\partial y}[B(\mathbf{U})\mathbf{E}] = -\mathbf{r}(\mathbf{U}). \tag{29}$$

This is a linear hyperbolic system of equations for the error vector with an extra error source term given as the negative of the residual $-\mathbf{r}(\mathbf{U})$.

As demonstrated in Refs. [6,7], the modified equation approach can be used for approximating the error source $-\mathbf{r}(\mathbf{U})$ for Eq. (29). For two-dimensional problems using the first-order Roe's upwind scheme, the error source vector in the ith control volume V_i may be estimated as

$$-\mathbf{r}_i = -\frac{1}{2V_i} \sum_{j \in \mathscr{I}_i} \left(I - c\frac{|\tilde{A}_j n_x^j + \tilde{B}_j n_y^j|}{\max_l(\max_k |\lambda_l^k|)} \right) |\Delta(\mathbf{f}_j n_x^j + \mathbf{g}_j n_y^j)| \tag{30}$$

for unsteady computations, and

$$-\mathbf{r}_i = -\frac{1}{2V_i} \sum_{j \in \mathscr{I}_i} |\Delta(\mathbf{f}_j n_x^j + \mathbf{g}_j n_y^j)| \tag{31}$$

for steady-state computations. In (30) and (31), $\mathbf{n} = (n_x, n_y)$ is the outward normal unit vector of the control volume interface, c the CFL number, I the unit matrix, $|\Delta(\mathbf{f}_j n_x^j + \mathbf{g}_j n_y^j)|$ the upwinding term in the flux vector of Roe's scheme, λ_l^k the kth ($k = 1, 2, 3, 4$) eigenvalue of the combined Jacobian matrix $\tilde{A}_j n_x^j + \tilde{B}_j n_y^j$ at the lth control volume and

$$\mathscr{I}_i = \{j \mid \text{the } j\text{th edge of control volume } i\}.$$

For steady-state computations, the matrices $A(\mathbf{U})$, $B(\mathbf{U})$ and the error source $-\mathbf{r}(\mathbf{U})$ are computed only once. Hence the computational cost for their evaluation is very small.

For boundary value problems, the boundary conditions need to be specified. In this paper, the boundary conditions are specified in ghost cells by imposing values or extrapolating from internal cells using the local characteristics.

Note that the matrix $(\tilde{A}n_x + \tilde{B}n_y)$ can be diagonalized as

$$\tilde{A}n_x + \tilde{B}n_y = LDR$$

with $D = \text{diag}(\lambda^1, \lambda^2, \lambda^3, \lambda^4)$, and where L and $R\,(= L^{-1})$ are formed from the left and right eigenvectors of the matrix, respectively.

First, for all boundary cells, the characteristic error variables $R\mathbf{E}$ are computed according to:

$$[R\mathbf{E}]^k_{\text{inlet}} = \begin{cases} 0 & \text{(analytic)} & \text{for } \lambda^k \geqslant 0, \\ [R\mathbf{E}]^k_{\text{int}} & \text{(extrapolate)} & \text{otherwise} \end{cases} \tag{32}$$

and

$$[R\mathbf{E}]^k_{\text{outlet}} = \begin{cases} 0 & \text{(analytic)} & \text{for } \lambda^k \leqslant 0, \\ [R\mathbf{E}]^k_{\text{int}} & \text{(extrapolate)} & \text{otherwise}, \end{cases} \tag{33}$$

where $[R\mathbf{E}]^k_{\text{int}}$ is the value at the internal neighboring cell.

Then the values for the error variables in the image cells are obtained as:

$$\mathbf{E} = L[R\mathbf{E}],$$

and $[R\mathbf{E}]$ is the boundary value as given in (32) for inlet and (33) for outlet, respectively.

6. Test cases

A comparison of the error estimation methods will be performed on four test cases, three of which possess closed form analytical solutions and the last of them is an NACA0012 transonic airfoil flow.

6.1. Subsonic radial flow

The first test case is an inviscid, isentropic, subsonic radial flow, as illustrated in Fig. 2. The flow inlet is located at the inner radius and the outlet at the outer radius. The left and bottom boundaries have been modeled as solid walls. The analytical solution is given as a transcendental equation for the Mach number M which varies only with the radius r, as follows:

$$f(M) = \frac{1}{\sqrt{\frac{1}{M^2} + \frac{\gamma-1}{2}}} \left[\frac{1}{1 + \frac{\gamma-1}{2}M^2} \right]^{1/(\gamma-1)} - \frac{1}{r} = 0. \tag{34}$$
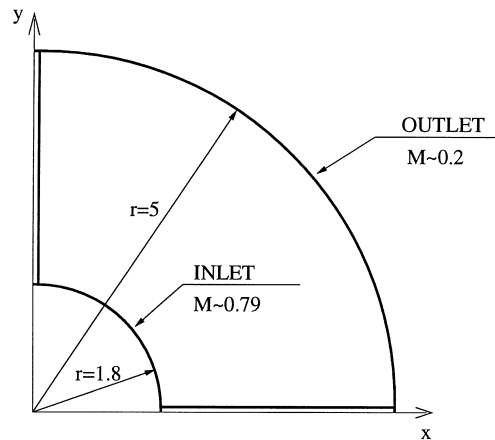
Fig. 2. Geometry for the subsonic radial flow.

The equation $f(M) = 0$ has been solved using an iterative Newton procedure. Once the Mach number is known, the isentropic relations are used to compute the remaining flow parameters.

6.2. Supersonic vortex flow

The second test case is an inviscid, isentropic, supersonic flow between concentric circular arcs, as illustrated in Fig. 3. The flow inlet is located at the right boundary and the flow exit is at the bottom boundary. The circular arcs are taken as solid walls. The inner radius has been taken as $r_{in} = 1$ and the outer radius as $r_{outer} = 1.384$. The flow is supersonic everywhere, with $M_{in} = 2.25$, $\rho_{in} = 1$, $p_{in} = 1/\gamma$ [11]. In a manner similar to that in radial flow, the flow parameters vary only with the radius r and are given by:

$$\rho(r) = \left[1 + \frac{\gamma - 1}{2} M_{in}^2 \left(1 - \left(\frac{r}{r_{in}} \right)^2 \right) \right]^{1/(\gamma - 1)}, \tag{35}$$

$$p(r) = \frac{1}{\gamma} \left[1 + \frac{\gamma - 1}{2} M_{in}^2 \left(1 - \left(\frac{r}{r_{in}} \right)^2 \right) \right]^{\gamma/(\gamma - 1)}, \tag{36}$$

$$T(r) = \frac{p(r)}{\rho(r)}, \quad c(r) = \sqrt{\gamma T(r)}, \quad u(r) = c(r) M(r) \frac{y}{r}, \quad v(r) = -c(r) M(r) \frac{x}{r}, \tag{37}$$

$$M(r) = \sqrt{\frac{k^2}{\frac{r}{r_{in}^2} - \frac{\gamma - 1}{2} k^2}}, \quad k = 1.586, \tag{38}$$

where ρ, p, T, M, c are the density, the pressure, the temperature, the Mach number and the sound speed, respectively.

6.3. Supersonic confluence

The third test case is a pure supersonic flow with two shocks and a slipline. The geometry of the problem is schematically illustrated in Fig. 4. In zones 3 and 4, the pressure is $p_3 = p_4 = 1.7238$ and the slipline between zones 3 and 4 makes an angle of $-0.745°$ with the horizontal direction. The oblique shock wave angles are $\beta_3 = 33.605°$ and $\beta_4 = 44.992°$, respectively.
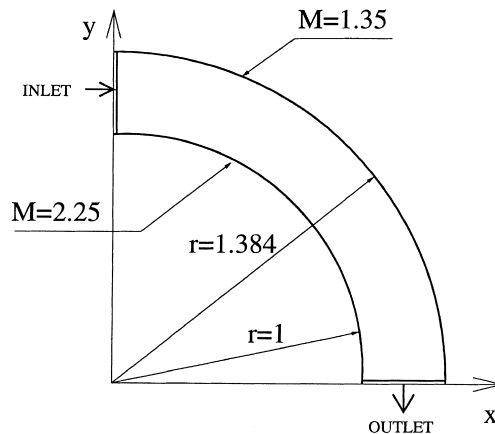
Fig. 3. Geometry for the supersonic vortex flow.
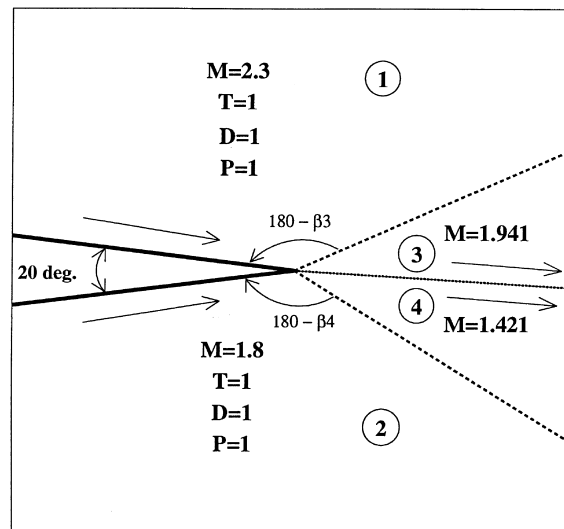
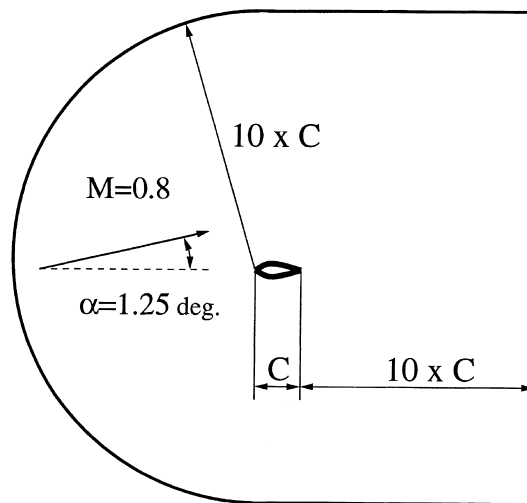Fig. 4. Analytical solution for the supersonic confluence flow.

Fig. 5. Geometry for the NACA0012 airfoil flow.

6.4. NACA0012 transonic airfoil flow

The last test case is a transonic airfoil flow. An NACA0012 airfoil is used with an incident *Mach* = 0.8 flow at an angle of 1.25°. A sketch of the configuration is given in Fig. 5. The flow produces a strong shock at the upper surface of the airfoil and a weaker shock at the lower surface. For the present computation, the outer boundary has been set at 10 chords from the airfoil.

7. Results

The results are divided into two groups: in the first group, presented in Figs. 7–10, the distributions of the local errors are shown, and this allows comparison of the exact error distribution with the estimated error distributions for the three first cases; in the second group, presented in Tables 1–10, the global errors are shown, and this allows a more quantitative analysis and comparison of the methods. Also given in the

Table 1
L_2 global norm of errors in density and estimation efficiency indices for the radial flow (first-order solutions on right triangular grids)

Grid	Exact error	Solution reconstruction		Richardson extrapolation		Error equation	
		Error	Eff. index	Error	Eff. index	Error	Eff. index
g_1	2.622e−2	8.474e−3	0.323	2.518e−2	0.960	1.467e−2	0.559
g_2	1.320e−2	4.431e−3	0.336	1.263e−2	0.957	7.585e−3	0.575
g_3	6.604e−3	2.277e−3	0.345	6.333e−3	0.959	3.844e−3	0.582

Table 2
L_2 global norm of errors in density and estimation efficiency indices for the radial flow (second-order solutions on right triangular grids)

Grid	Exact error	Solution reconstruction		Richardson extrapolation		Error equation	
		Error	Eff. index	Error	Eff. index	Error	Eff. index
g_1	7.561e−4	5.414e−4	0.716	9.198e−4	1.216	6.680e−4	0.883
g_2	1.797e−4	1.384e−4	0.770	2.233e−4	1.242	1.912e−4	1.064
g_3	4.446e−5	3.522e−5	0.792	5.419e−5	1.219	5.586e−5	1.256

Table 3
L_2 global norm of errors in density and estimation efficiency indices for the radial flow (first-order solutions on unstructured triangular grids)

Grid	Exact error	Solution reconstruction		Richardson extrapolation		Error equation	
		Error	Eff. index	Error	Eff. index	Error	Eff. index
g_1	2.317e−2	8.556e−3	0.369	2.299e−2	0.993	1.371e−2	0.592
g_2	1.198e−2	4.467e−3	0.373	1.195e−2	0.998	7.237e−3	0.604
g_3	6.119e−3	2.287e−3	0.374	6.214e−3	1.015	3.675e−3	0.601

Table 4
L_2 global norm of errors in density and estimation efficiency indices for the radial flow (second-order solutions on unstructured triangular grids)

Grid	Exact error	Solution reconstruction		Richardson extrapolation		Error equation	
		Error	Eff. index	Error	Eff. index	Error	Eff. index
g_1	1.095e−3	6.956e−4	0.635	1.435e−3	1.310	3.243e−3	2.962
g_2	2.773e−4	1.878e−4	0.677	3.496e−4	1.261	9.072e−4	3.272
g_3	6.335e−5	4.716e−5	0.744	8.518e−5	1.345	2.462e−4	3.886

Table 5
L_2 global norm of errors in density and estimation efficiency indices for the supersonic vortex flow (first-order solutions on right triangular grids)

Grid	Exact error	Solution reconstruction		Richardson extrapolation		Error equation	
		Error	Eff. index	Error	Eff. index	Error	Eff. index
g_1	1.382e−1	6.583e−2	0.476	1.211e−1	0.876	1.592e−1	1.152
g_2	6.835e−2	3.314e−2	0.485	5.632e−2	0.824	7.464e−2	1.092
g_3	3.547e−2	1.666e−2	0.470	2.619e−2	0.738	3.730e−2	1.052

Table 6
L_2 global norm of errors in density and estimation efficiency indices for the supersonic vortex flow (second-order solutions on right triangular grids)

Grid	Exact error	Solution reconstruction		Richardson extrapolation		Error equation	
		Error	Eff. index	Error	Eff. index	Error	Eff. index
g_1	3.786e−3	1.063e−3	0.281	3.979e−3	1.051	1.339e−3	0.354
g_2	8.451e−4	2.680e−4	0.317	8.564e−4	1.013	3.777e−4	0.447
g_3	2.168e−4	7.100e−5	0.327	1.844e−4	0.850	1.006e−4	0.464

Table 7
L_2 global norm of errors in density and estimation efficiency indices for the supersonic confluence flow (first-order solutions on unstructured triangular grids)

Grid	Exact error	Solution reconstruction		Richardson extrapolation		Error equation	
		Error	Eff. index	Error	Eff. index	Error	Eff. index
g_1	7.078e−2	1.719e−2	0.243	1.175e−1	1.66	5.345e−2	0.755
g_2	5.332e−2	1.143e−2	0.214	8.856e−2	1.66	4.754e−2	0.892
g_3	3.857e−2	8.029e−3	0.208	6.679e−2	1.73	3.616e−2	0.937

Table 8
L_2 global norm of errors in density and estimation efficiency indices for the supersonic confluence flow (second-order solutions on unstructured triangular grids)

Grid	Exact error	Solution reconstruction		Richardson extrapolation		Error equation	
		Error	Eff. index	Error	Eff. index	Error	Eff. index
g_1	4.883e−2	8.418e−3	0.172	1.331e−1	2.726	1.610e−2	0.330
g_2	3.564e−2	5.487e−3	0.154	9.821e−2	2.756	1.145e−2	0.321
g_3	2.556e−2	3.821e−3	0.149	7.246e−2	2.835	7.511e−3	0.294

Table 9
L_2 global norm of errors in density for the NACA0012 airfoil flow (first- and second-order solutions on unstructured triangular grids)

Grid	Solution reconstruction		Richardson extrapolation		Error equation	
	First order	Second order	First order	Second order	First order	Second order
g_1	1.112e−2	4.509e−3	6.329e−2	8.383e−2	3.947e−2	7.056e−3
g_2	6.608e−3	2.322e−3	4.388e−2	7.031e−2	2.817e−2	6.811e−3
g_3	4.043e−3	1.722e−3	3.043e−2	5.897e−2	1.111e−2	4.788e−3

Table 10
Order of convergence obtained by Eq. (8) using the L_2 norms of the exact error (RTM = right triangular mesh, UTM = unstructured triangular mesh)

Test case	First order			Second order		
	g_1/g_2	g_2/g_3	g_1/g_3	g_1/g_2	g_2/g_3	g_1/g_3
Radial flow (RTM)	0.990	0.999	0.995	2.07	2.02	2.04
Radial flow (UTM)	0.951	0.969	0.960	1.98	2.13	2.06
Vortex flow (RTM)	1.016	0.946	0.981	2.16	1.96	2.06
Confluence flow (UTM)	0.409	0.467	0.438	0.45	0.48	0.47

tables is the efficiency index, which is simply the ratio of predicted error over exact error. For each problem, a set of three triangular grids denoted g_1, g_2, g_3 has been created with the same relative grid concentration and with refinement factors of $r \approx t^{(2)}/t^{(1)} \approx t^{(3)}/t^{(2)} \approx 2$. Fig. 6 presents the coarsest of the structured and unstructured grids that have been used in this study.

(a) Radial flow (1248 elements)

(b) Supersonic vortex flow (300 elements)

(c) Supersonic confluence flow (2500 elements)

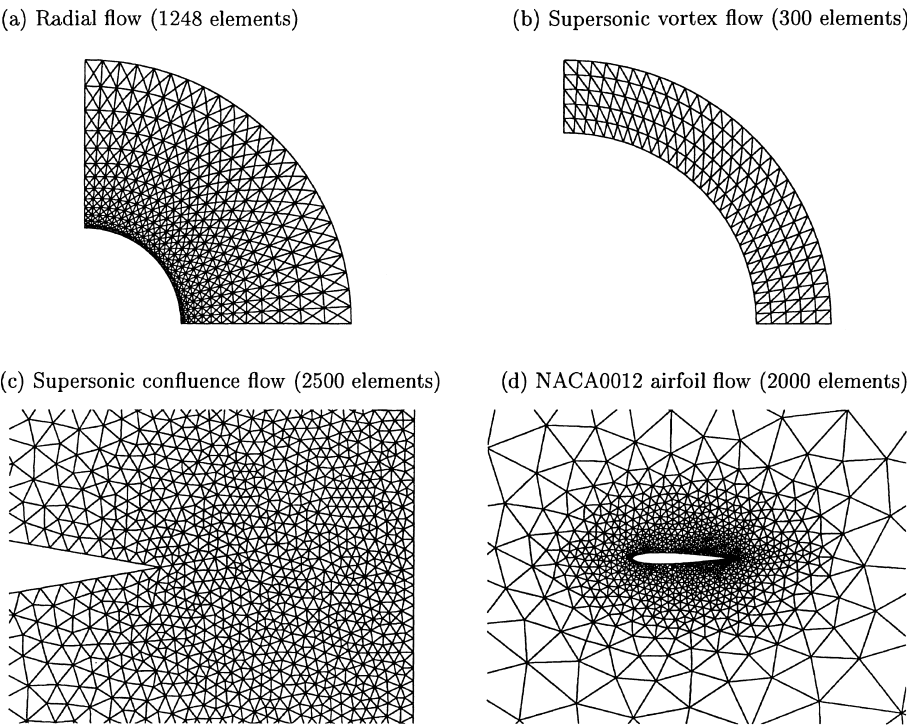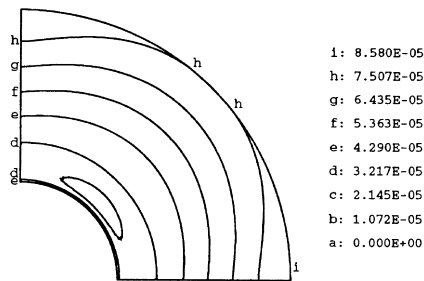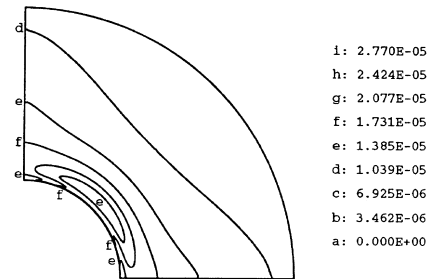(d) NACA0012 airfoil flow (2000 elements)

Fig. 6. Grids used for the radial flow (coarsest structured grid), the supersonic vortex flow (coarsest structured grid), the supersonic confluence flow (coarsest unstructured grid) and the NACA0012 airfoil flow (coarsest unstructured grid).
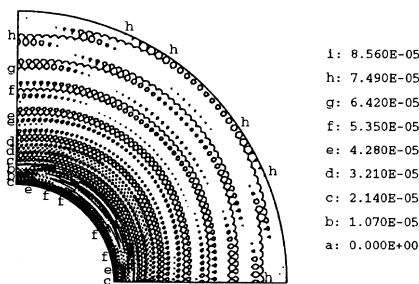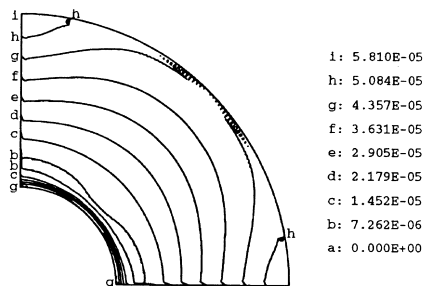
(a) Exact Error

(b) Solution Reconstruction

```
i: 8.580E-05
h: 7.507E-05
g: 6.435E-05
f: 5.363E-05
e: 4.290E-05
d: 3.217E-05
c: 2.145E-05
b: 1.072E-05
a: 0.000E+00
```

```
i: 2.770E-05
h: 2.424E-05
g: 2.077E-05
f: 1.731E-05
e: 1.385E-05
d: 1.039E-05
c: 6.925E-06
b: 3.462E-06
a: 0.000E+00
```

(c) Richardson Extrapolation

(d) Error Equation

```
i: 8.560E-05
h: 7.490E-05
g: 6.420E-05
f: 5.350E-05
e: 4.280E-05
d: 3.210E-05
c: 2.140E-05
b: 1.070E-05
a: 0.000E+00
```

```
i: 5.810E-05
h: 5.084E-05
g: 4.357E-05
f: 3.631E-05
e: 2.905E-05
d: 2.179E-05
c: 1.452E-05
b: 7.262E-06
a: 0.000E+00
```

Fig. 7. L_2 local norm distributions of error in density for the radial flow (first-order solutions on right triangular grids).

7.1. Subsonic radial flow

Let us first consider the radial flow problem, the results of which are shown in Fig. 7 and Tables 1–4. Fig. 7 illustrates the local distribution of the exact and estimated errors in density for the first-order scheme on the finest of the right triangular grids.

For such a smooth flow, Richardson extrapolation provides a fairly accurate error distribution, correctly capturing the location and the magnitude of the error. The method is a little noisy, this noise coming from the interpolation of the medium solution on the fine grid required to obtain a measure of the difference in solutions. No special filtering has been used to reduce the noise since the distribution is already convincing and filtering could alter the performance of the method.

The error equation method also performs rather well, especially in the representation of the distribution of the largest errors close to the flow outlet. The method slightly underestimates the maximum error value, but this is a known property of the method.

The error distribution obtained with the reconstruction method is very poor. As expected, this method predicts the maximum error to occur at the flow inlet where the solution gradient is the highest. However, this is not the location of the maximum of the exact error. It is believed that the reconstruction method, being based only on the computation of interpolation errors, is unable to capture the other kinds of errors, or error convection or accumulation, typical of hyperbolic problems.

Tables 1–4 report the global error obtained with the three methods for first- and second-order schemes on right triangular and unstructured grids. The tendencies are similar for both types of meshes and for both schemes. Richardson extrapolation always provides the best estimation, followed by the error equation technique. The solution reconstruction method yields a fair efficiency index, but considering the bad local error distribution shown in Fig. 7, it is not clear whether this fair result is reliable or only accidental.

As discussed previously in the presentation of Richardson extrapolation, the order of convergence of the scheme can be computed and is shown in Table 10. For the radial flow problem on right triangular or
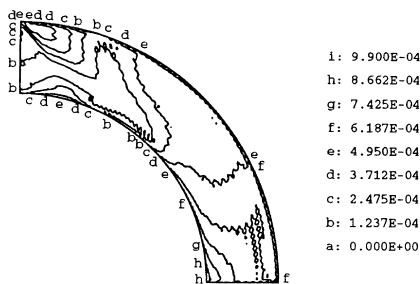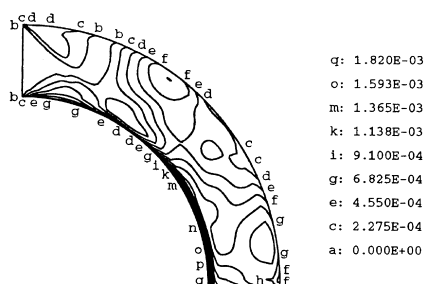
(a) Exact Error
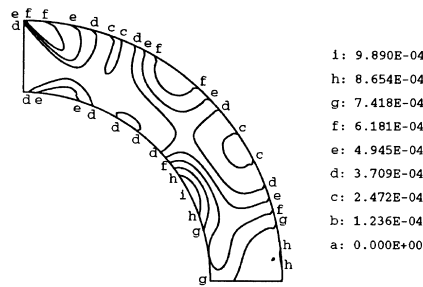
(b) Solution Reconstruction
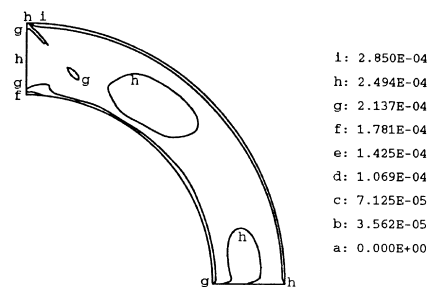
(c) Richardson Extrapolation

(d) Error Equation

Fig. 8. L_2 local norm distributions of error in density for the supersonic vortex flow (first-order solutions on right triangular grids).

unstructured grids, the scheme order approaches the formal order of the scheme very well, which was expected for such a smooth flow.

7.2. Supersonic vortex flow

The results for the second test case are shown in Fig. 8 and in Tables 5 and 6. Fig. 8 illustrates the local distribution of the exact and computed errors in density for the first-order scheme on right triangular grids.

For this supersonic case, the three error estimation methods perform qualitatively in the same way as for the previous subsonic case. The error distribution and magnitude obtained from Richardson extrapolation is very accurate. Some noise is still present, again attributable to solution transfer. The prediction obtained with the error equation method is very good. However, an accumulation of the error is observed at the inner radius which can be attributed to the solver used for the error equation [16]. The solution reconstruction technique misses most of the error distribution, as well as the error magnitude.

Tables 5 and 6 present the global errors measured in the L_2 norm for the first- and second-order solutions, respectively. For the first-order solutions, the efficiency indices obtained with Richardson extrapolation and with the error equation method are very good. The efficiency of the reconstruction method is reasonable, but again this is not representative since the error distribution is wrong. For the second-order scheme, Richardson extrapolation performs best. The error equation method underestimates the error peaks, this being attributable to the method used to solve the error equation. A higher-order solution might be required to obtain better results, but the performance of the method is still reasonable.

7.3. Supersonic confluence

Let us now consider the third test case, which contains flow discontinuities. The distributions of the local errors are shown in Fig. 9 for the first-order scheme. This is a very simple case and the methods perform

(a) Exact Error

(b) Solution Reconstruction

o: 1.529E-03
m: 1.311E-03
k: 1.092E-03
i: 8.738E-04
g: 6.554E-04
e: 4.369E-04
c: 2.185E-04
a: 0.000E+00

o: 3.680E-04
m: 3.154E-04
k: 2.629E-04
i: 2.103E-04
g: 1.577E-04
e: 1.051E-04
c: 5.257E-05
a: 0.000E+00

(c) Richardson Extrapolation

(d) Error Equation

o: 2.342E-03
m: 2.007E-03
k: 1.673E-03
i: 1.338E-03
g: 1.004E-03
e: 6.691E-04
c: 3.345E-04
a: 0.000E+00

o: 1.380E-03
m: 1.183E-03
k: 9.857E-04
i: 7.886E-04
g: 5.914E-04
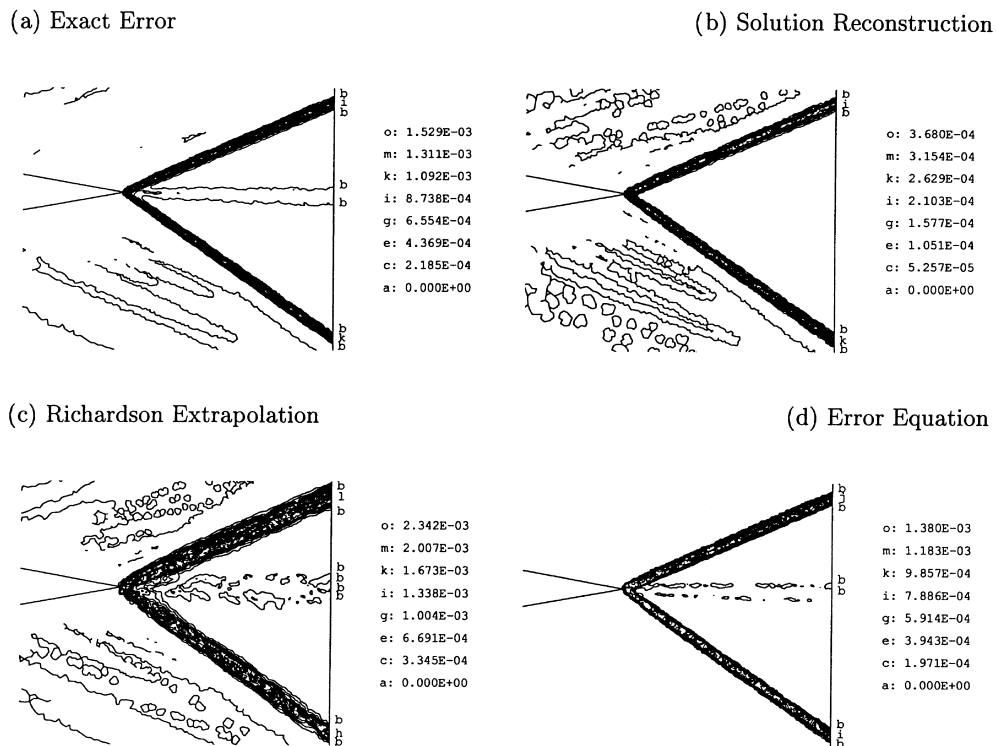e: 3.943E-04
c: 1.971E-04
a: 0.000E+00

Fig. 9. L_2 local norm distributions of error in density for the supersonic confluence flow (first-order solutions on unstructured triangular grids).

well qualitatively. If we look more carefully at the details of the distributions, Richardson extrapolation overpredicts the error magnitude, as well as the width of the error distribution around the shocks. This is due to the transfer of the solution from the medium grid on which the shock is wider. This behavior should be expected with this method since it is based on the smoothness of the solution which is not the case for such discontinuities. The solution reconstruction method predicts correctly the location of the error, but underpredicts its magnitude by a factor of four. The error equation performs rather well both in location and magnitude. Note also that the small errors located near the slipline are well captured by the methods based on Richardson extrapolation and on error equation but are completely absent from the results of the reconstruction technique. For such a flow, with pure discontinuities, the solver is shown (in Table 10) to converge with an order of convergence of 0.5, almost independently of the order of the scheme.

Tables 7 and 8 present the global errors for this third test case. As discussed for the local distributions, Richardson extrapolation overpredicts the error in all cases, the solution reconstruction method provides the less accurate prediction and the error equation method is fairly good, especially for the first-order scheme. The grid refinement is shown to improve the efficiency index close to one. It should be noted that for the second-order scheme, a third-order solution of the error equation is recommended, but has not been used in the present work. This could improve the performance of this method for all the second-order cases.

7.4. NACA0012 airfoil flow

Fig. 10 presents the computed density distribution on the finest grid, together with a comparison of the errors estimated with the three techniques. Note that the maximum value of the error scale has been set to a lower value for the solution reconstruction technique, so that is possible to distinguish the error distribution. Note also that for the three error plots, the elements with an error larger than the maximum shown have been colored in red.
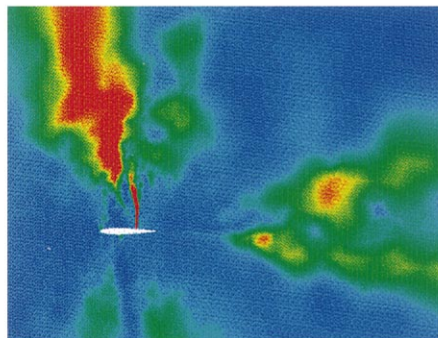
(a) Density distribution
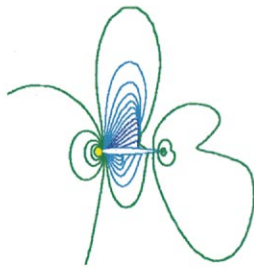
(b) Solution Reconstruction
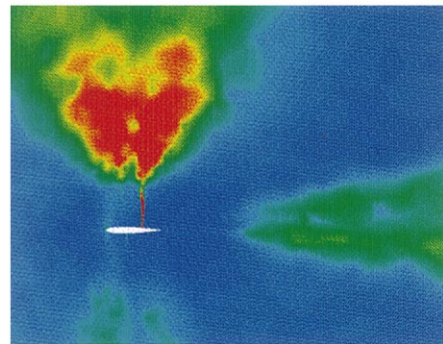
(c) Richardson Extrapolation

(d) Error Equation
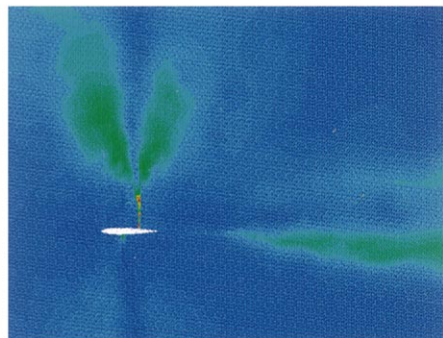
Fig. 10. Density distribution and L_2 local norm distributions of error in density for the NACA0012 airfoil flow (first-order solutions on unstructured triangular grids).

For the three error estimators, most of the errors are concentrated across the upper shock wave. Errors at the lower weak shock wave are also captured. Large errors are predicted above the airfoil where the grid becomes very coarse, and in the wake for the same reason. Compared with the previous test cases, the solution reconstruction technique behaves qualitatively in a more reasonable way for this problem, but again predicts much smaller errors than the other two methods. The convergence rate of the scheme has also been computed for this case based on the three solutions computed with 2000, 8000 and 32 000 elements. For the first-order scheme, a rate of 0.53 has been obtained, while a rate of only 0.25 was obtained for the second-order scheme. These predicted rates demonstrate that, for complex cases, various effects can affect the convergence rate in a negative way. It is believed that the transonic nature of the flow, and mainly the convergence of the location of the shock waves, is responsible for this slow convergence rate.

Table 9 presents the global L_2 norms of error in density for the first- and second-order schemes. For the first-order scheme, the error equation technique and Richardson extrapolation predict the same level of error, while the solution reconstruction technique underestimates the error. For the second-order scheme, the results are more difficult to analyze because of the apparent low rate of grid convergence. As a result, Richardson extrapolation predicts higher global errors than for the first-order solutions, which is not reasonable. However, the solution reconstruction and error equation techniques are more consistent. The fact that the solution is not differentiable at the shock and the sensitivity of the shock location on the grid are believed to be the causes of the problems.

8. Conclusion

Three techniques for obtaining error estimates for finite-volume solutions have been compared in this study. The three techniques are: a solution reconstruction technique which provides a measure of the interpolation error; Richardson extrapolation which requires the solution on at least two different grids; and the error equation method which solves an equation for the error distribution with source terms approximated from the discretization error of the scheme.

The three techniques were first compared for smooth subsonic and supersonic flows with known analytical error distributions. It was shown that for such smooth flows, Richardson extrapolation provides the more accurate error estimates, followed by the error equation method. The solution reconstruction technique was shown to provide false error distributions, as well as global error predictions that are too low.

The techniques were then compared for a pure supersonic flow with discontinuities. In this case, Richardson extrapolation, which assumes smoothness of the solution with the grid refinement, consistently overpredicts the exact error. The error equation method performs very well for the first-order scheme, but its performance degrades for the second-order scheme. A third-order solution of the error equation may be required to improve its performance.

In a last test case, a transonic flow was computed to compare the error estimation methods. No exact solution was available and no attempt was made to approximate it. The idea was rather to show the spectrum of results that could be obtained in a realistic case. All methods have predicted dominant errors to be located at the upper shock and this is probably the case. However, difficulties inherent to transonic airfoil flows, such as the prediction of the location of the shocks and their extent, strongly affect the grid convergence of the scheme. Finer grids will be required to approach the asymptotic region, adapted grids being a good candidate. Also, it is believed that shock-fitting methods, as in Ref. [17], could improve the grid convergence rate for cases with discontinuities, but more work is required to investigate this point.

Acknowledgements

References

[1] P.J. Roache, Perspective: A method for uniform reporting of grid refinement studies, J. Fluids Engrg. 116 (1994).

[2] P.J. Roache, Verification of codes and calculations, in: AIAA – 26th Aerospace Sciences Meeting and Exhibit, San Diego, CA, US, AIAA-95-2224.

[3] O.C. Zienkiewicz, J.Z. Zhu, A simple error estimator and adaptive procedure for practical engineering analysis, Int. J. Num. Meth. Engrg. 24 (1987) 337–357.

[4] J.A. Peraire, M. Vahdati, K. Morgan, O.C. Zienkiewicz, Adaptive remeshing for compressible flow computations, J. Comput. Phys. 72 (1987) 449–466.

[5] A. Ilinca, J.-Y. Trépanier, R. Camarero, Error estimator and adaptive moving grids for finite volumes schemes, AIAA J. 33 (11) 1995.

[6] X.D. Zhang, J.-Y. Trépanier, R. Camarero, A posteiori error estimation for finite-volume solutions of hyperbolic conservation laws, CERCA Technical Report R97-16, 1997; also submitted to Comput. Meth. Appl. Mech. Engrg..

[7] X.D. Zhang, J.-Y. Trépanier, R. Camarero, An a posteriori error estimation method based on an error equation, in: Proceedings of the AIAA 13th Computational Fluid Dynamics Conference, Snowmass, CO, US, AIAA-97-1889, 1997.

[8] P.L. Roe, Approximated Riemann solvers, parameter vectors and difference scheme, J. Comput. Phys. 43 (1981).

[9] J.-Y. Trépanier, M. Reggio, H. Zhang, R. Camarero, A finite-volume method for the Euler equations on arbitrary lagrangian–eulerian grids, Computers and Fluids 20 (4) (1991) 399–409.

[10] T.-J. Barth, Recent developments in high order K-exact reconstruction on unstructured meshes, AIAA Paper, January 1993.

[11] M. Aftosmis, D. Gaitonde, T. Sean Tavares, On the accuracy, stability and monotonicity of various reconstruction algorithms for unstructured meshes, in: AIAA – 32nd Aerospace Sciences Meeting and Exhibit, Reno, NV, US, AIAA-94-0415, 1994.

[12] C. Ilinca, J.-Y. Trépanier, Grid convergence studies and error estimates for the Euler equations on unstructured grids, in: Proceedings of the AIAA 13th Computational Fluid Dynamics Conference, Snowmass, CO, US, AIAA-97-1890, 1997.

[13] C.F. Ollivier-gooch, A new class of ENO schemes based on unlimited data-dependent least-squares reconstruction, in: AIAA – 34th Aerospace Sciences Meeting and Exhibit, Reno, NV, US, AIAA-96-0887, 1996.

[14] K.A. Hoffmann, Computational fluid dynamics for engineers, Engrg. Education System, Austin, TX, US, 1989.

[15] G.H. Klopfer, D.S. Mcrae, Nonlinear truncation error analysis of finite difference schemes for the Euler equations, AIAA J. 21 (4) (1983) 487–494.

[16] X.D. Zhang, J.-Y. Trépanier, M. Reggio, A. Benmeddour, R. Camarero, Grid influence on upwind schemes for the Euler and Navier–Stokes equations, AIAA J. 34 (4) (1996) 717–727.

[17] J.-Y. Trépanier, M. Paraschivoiu, M. Reggio, R. Camarero, A conservative shock fitting method on unstructured grids, J. Comput. Phys. 126 (1996) 421–433.